On the elastic moduli of three-dimensional assemblies of spheres: characterization and modeling of fluctuations in the particle displacement and rotation

Ivana Agnolin, Jean-Noël Roux

▶ To cite this version:

On the elastic moduli of three-dimensional assemblies of spheres: characterization and modeling of fluctuations in the particle displacement and rotation

I. Agnolin, J.-N. Roux

Laboratoire des Matériaux et des Structures du Génie Civil*
Institut Navier, 2 allée Kepler, Cité Descartes, 77420 Champs-sur-Marne, France

Abstract

The elastic moduli of four numerical random isotropic packings of Hertzian spheres are studied. The four samples are assembled with different preparation procedures, two of which aim to reproduce experimental compaction by vibration and lubrication. The mechanical properties of the samples are found to change with the preparation history, and to depend much more on coordination number than on density.

Secondly, the fluctuations in the particle displacements from the average strain are analysed, and the way they affect the macroscopic behavior analyzed. It is found that only the average over equally oriented contacts of the relative displacement these fluctuations induce is relevant at the macroscopic scale. This average depends on coordination number, average geometry of the contact network and average contact stiffness. As far as the separate contributions from particle displacements and rotations are concerned, the former is found to counteract the average strain along the contact normal, while the latter do in the tangential plane. Conversely, the tangential components of the center displacements mainly arise to enforce local equilibrium, and have a small, and generally stiffening effect at the macro-scale.

Finally, the fluctuations and the shear modulus that result from two approaches available in the literature are estimated numerically. These approaches are both based on the equilibrium of a small-sized representative assembly. The improvement of these estimate with respect to the average strain assumption indicates that the fluctuations relevant to the macroscopic behavior occur with short correlation length.

Keywords: Granular material, elastic material, constitutive behavior, contact mechanics, wave propagation

---

1 Introduction

Granular media are relevant to civil engineering in the form of soils or granulates; to agriculture as seeds; to industry as powders to compact or mix, or because they represent a convenient way to shape materials that are to store or transport. Granular media are made of grains that interact at contact points, where forces arise to oppose the relative displacement between contacting particles. The focus in this work is on the stress-strain relationship for dense assemblies in the linear elastic regime. This concerns the reversible response to small disturbances, with the additional constraint that any change on the geometry of the contact network be negligible. Experimentally, this range is investigated by wave propagation, or by biaxial tests when the technical apparatus allows to measure very small deformations, as in Thomann and Hryciw (1990) and Hicher (1996).

The response of granular media crucially depends on the structure of the contact network. This is defined by the average number of contacts per particle and the texture fabric, and depends on the procedure employed to assemble the sample. Current assembling procedures consist in shakes, taps, vibration, lubrication or undulatory shear, as in Nicolas et al. (2000), Jia and Mills (2001) or Cundall et al. (1989). In two-dimensions the particle fabric is accessible, classically through experiments on photoelastic disks like those in Majmudare and Behringer (2005) and Atman et al.) 2005. Photoelastic disks allow detection of contacts through that of colored fringes on the surface of interacting grains, and computation of the contact forces through image analysis. On the contrary, the unambiguous identification of the contact network in three dimensions still represents an unsolved task, due to the difficulty to distinguish between infinitely close and contacting grains. Even when advanced techniques are used, like X-Ray tomography in Aste et al. (2005), the uncertainty in the determination of the number of neighbors remains significant. As a consequence, the assemblies are still customarily characterized in terms of density, which is the only easily-measured quantity related to the microstructure. Density still plays a central role in the studies about granular media, especially in the context of compaction (for example, Procopio and Zavanglios, 2005) or in Cam-Clay-like models (Roscoe and Burland, 1968). Numerical simulations are at present the only tool to access the internal structure. Discrete Element Method (DEM) simulations are currently employed, which predict the evolution of a granular assembly by integration in time of the equations of motion of the individual particles (Cundall and Strack, 1979). These are treated as rigid bodies that interact at contact points, thereby neglecting the deformation of the grains as continua and the mutual influence between close contacts on the same grain. Such an assumption is reasonable in three dimensions, where the elastic deformation induced by the force between contacting bodies decays as the square of the distance from the contact surface (Johnson, 1985). In two dimensions, the decay is only proportional to this distance. In Procopio and Zavaliangos (2005) two-dimensional assemblies of disordered glass disks are simulated by using both a DEM code and a Finite Element Method (FEM) mesh for the individual particles. Comparison between the two simulations shows that incorporating the behavior of the

beads as continua does soften the assembly. Like in experiments, the first operation in a numerical simulation is sample compaction. In the scientific coomunity, this is almost exclusively performed by means of a frictionless compression, which is easy to reproduce and allows to match experimental densities. A recent study by Makse et al. (2004) suggests that the behavior of numerical samples assembled in this way is in agreement with that of real assemblies of glass beads under large pressures, between 10 and 100 MPa. However, to our knowledge neither alternative procedures nor the sample behavior in a smaller pressure range, though recurrent in geotechnical tests, have been sufficiently studied.

In Continuum Mechanics, the interest is in the prediction of the elastic moduli. A classic attempt follows from assuming that the relative displacements between grains are those induced by the average strain. In this way, Digby (1981) and Walton (1987) analytically infer the bulk and shear modulus of a random assembly of spheres. Comparison with the elastic moduli of numerical assemblies, as in Cundall et al. (1989), reveals that the prediction of the bulk modulus is sufficiently accurate, while that of the shear modulus is severely overestimated. The average strain assumption fails because it does not incorporate considerations of equilibrium, which is attained by the grains at the expenses of additional displacement fluctuations in the presence of disorder. In fact, forces and torques induced by the average strain identically balance only in perfectly ordered packings. This apparently conflicts with the experiments in Duffy and Mindlin (1957) on regular packs of steel spheres, which still exhibit a shear modulus different from the average strain prediction, especially at low pressure. Goddard (1990) proposes as an explanation the squeezing of conical asperities to Herztian contacts and the buckling of compressed columns, which are mechanisms that imply a significative evolution of the contact network. However, the work of Velicky and Caroli (1999) on hexagonal two-dimensional assemblies of spheres shows that even small dispersions in the diameter induce important deviations from the average strain prediction.

Several analytical solutions in the literature attempt to overcome the insufficiency of the average strain assumption. Some focus on contact forces. For example, Chang et al. (1995) estimate the elastic moduli of assemblies of frictional spheres whose contact forces are made depend on the average fabric. They show that the moduli depend on the ratio between tangential and normal contact stiffness and on the geometry of the fabric tensor. The same is done in Trentadue (2003), but in the more general context of non-spherical particles. Other approaches focus on displacements, solving for them the balance of force and torque on a small-sized subassembly. This is the case in the Pair Fluctuation (PF) method in Jenkins and La Ragione (2001), and in the 1-Fluctuating Particle (1FP) method in Kruyt and Rothenburg (2002). These methods have been applied to estimate, in turn, the shear modulus of dense assemblies of frictionless spheres and of non-rotating frictional disks. With respect to the average strain assumption, the ratio of the estimate to the effective value is reduced from 40 to 5 in the first case, and gets close to 1 in the second case.

The performance of a prediction depends on how realistic its assumptions are with respect to experimental observations. In two dimensions, the numerical simulations

of Calvetti and Emeriault (1999) and Kruyt and Rothenburg (2001) show that the average force over equally oriented contacts obeys the directional dependence predicted by the average strain assumption. That is, isotropic deformations induce isotropic fluctuations on average, while a biaxial compression induces radial fluctuations that are largest in the direction of the maximal compression and tangential ones that are largest at 45 degrees from the principal strains. The two-dimensional simulation in Kuhn (1999) reveals the appearance of deformation patterns. Gaspar and Koenders (2001) reexamine this simulation and relate the width of the deformation patterns to the correlation length of displacement fluctuations, which is found to be of about five particle diameters. Agnolin and Kruyt (2006) examine the linear elastic behavior of frictional assemblies of disks of coordination number between 3.5 and 5, and estimate their shear modulus in the hypothesis that the displacement fluctuations correlate over four particle diameters. With respect to the average strain assumption, they obtain a decrease in the ratio of the estimate to the effective value from more than 3 to about 1.5 in the less favorable case, which corresponds to small coordination number. Other simulations report much wider correlation lengths. In the 2D simulation in Williams and Rege (1997) displacement fluctuations occur in circulations cells that span a length of about twenty-particles. So large correlation lengths are likely to be induced by the large deformation applied and to be further emphasised by the particle softness. In this simulation, the deformation reaches 10% of particle diameter in steps of 1% of particle diameter, which are values characteristic of peack and post-peak behavior in both experiments on sand and numerical simulations of glass spheres (Thornton and Antony, 1998). A thorough description of the fluctuations from the average strain from experiments or numerical simulations and of the way they determine the macroscopic behavior is still missing in three dimensions.

In this work, a series of numerical isotropic assemblies of glass beads is first created. The beads interact through Hertzian contact forces, whose constitutive law results in an increase of the particle stiffness with the overlap. Each sample is compacted following a different preparation procedure, and among the procedures, two aim to reproduce experimental compaction. All procedures result in similar densities at the same pressure, but in significantly different coordination number. The elastic moduli of the samples are determined over a wide range of pressure, and compared with their estimate on the base of the average strain assumption. The fluctuations from the average strain the samples undergo are characterized, and conclusions are derived about the way they determine the behavior of the equivalent continuum. In doing so, distinction is made between the contributions from the various kinematic ingredients, namely center displacements and rotations, which are inherent in the discrete nature of granular materials. Finally, two approaches available in the literature are discussed and compared, which predict fluctuations consistent with our experimental observations. Our study fixes the performance attainable by analytical solutions that would be proposed to these approaches for frictional spheres, and concludes about the size of the smallest domain which needs to be considered to reliably predict the fluctuations relevant to the macroscopic behavior.

2 Micromechanics

The simulated grains are glass beads of diameter D and mass m, and are treated as rigid bodies that interact through points of contact. A contact between two grains, say i and j, is defined by its position and the unit vector $\mathbf{n}^{(ij)}$ that points from the center of grain i to that of grain j. In a counterclockwise Cartesian reference frame of axes $\mathbf{e}_1$, $\mathbf{e}_2$, $\mathbf{e}_3$,

$$\mathbf{n}^{(ij)} = (\cos\theta, \;\sin\theta\cos\phi, \;\sin\theta\sin\phi),$$

where θ is the polar angle with respect to axis 1, and ϕ is the azimuthal angle. Let $\mathbf{u}^{(i)}$ and $\mathbf{u}^{(j)}$ be the displacement of the two grains; $\boldsymbol{\omega}^{(i)}$ and $\boldsymbol{\omega}^{(j)}$ their rotation; $\mathbf{u}^{(ij)}$ their relative displacement, and $\mathbf{t}^{(ij)}$ the unit vector aligned with the tangential component $\mathbf{s}^{(ij)}$ of $\mathbf{u}^{(ij)}$; $\mathbf{s}^{(ij)}$ has absolute value $s^{(ij)}$, i.e.

$$
\begin{aligned}
\mathbf{u}^{(ij)} &= \mathbf{u}^{(i)} - \mathbf{u}^{(j)} + \frac{D}{2}\left[\boldsymbol{\omega}^{(i)} + \boldsymbol{\omega}^{(j)}\right] \times \mathbf{n}^{(ij)}, \\
\mathbf{s}^{(ij)} &= \mathbf{u}^{(ij)} - u_a^{(ij)} n_a^{(ij)} \mathbf{n}^{(ij)}, \\
s^{(ij)} &= |\mathbf{s}^{(ij)}|, \\
\mathbf{t}^{(ij)} &= \mathbf{s}^{(ij)}/s^{(ij)},
\end{aligned}
$$

where the symbol $\times$ and the vertical bars $|...|$ denote, in turn, the vector product and the absolute value. Contacting grains interact by means of contact forces. These oppose their relative displacement at the contact point, and have normal and tangential component to the contact of absolute value $F_N^{(ij)}$ and $F_T^{(ij)}$, respectively. $F_N^{(ij)}$ obeys Hertz's law, i.e.

$$F_N^{(ij)} = \frac{Y\sqrt{D}h^{(ij)3/2}}{(1-\nu^2)3}, \tag{1}$$

where Y is the Young's modulus of the material the beads are made of, ν is its Poisson's modulus and $h^{(ij)}$ is the contact overlap. No tensile normal forces are allowed. The increments in $F_T^{(ij)}$ obey

$$dF_T^{(ij)} = \frac{2(1-\nu)}{2-\nu}\frac{dF_N^{(ij)}}{dh^{(ij)}}ds^{(ij)}, \tag{2}$$

which is Mindlin's (Mindlin and Deresiewicz, 1953) initial tangential stiffness between two spheres kept in contact by the normal force $F_N^{(ij)}$. $F_T^{(ij)}$ is bounded above by the coefficient of friction μ, so that $|F^T| \leq \mu|F^N|$. Along some loading-unloading paths (Elata and Berryman, 1996), use of (2) might induce spurious creation of energy, which is avoided by incorporating the recommendations by Johnson and Norris (1996). The contact force $\mathbf{F}^{(ij)}$ of grain j on grain i can thus be written as

$$F_r^{(ij)} = -F_N^{(ij)} n_r^{(ij)} - F_T^{(ij)} t_r^{(ij)}.$$

At the macroscopic level, the assembly is characterised by its solid fraction Φ and coordination numbers z and z^*, namely

$$
\begin{aligned}
\Phi &= \frac{N\pi D^3}{6V}, \\
z &= \frac{2C}{N}, \\
z^* &= \frac{2C}{N_{act}},
\end{aligned}
\tag{3}
$$

where N is the number of grains in the assembly, N_{act} is that of force-carrying grains and C is the number of contacts. The average number of contacts per active particle z^* emphasises the role of the force-carrying network. One has that $z = z^* N_{act}/N$. The macroscopic stress σ_{rm} in a numerical assembly (Cundall, 1983) is given by

$$
\sigma_{rm} = -\frac{D}{2V} \sum_{i=1}^{N_{act}} \sum_{j=1}^{N(i)} F_r^{(ij)} n_m^{(ij)},
\tag{4}
$$

which is the average over the volume V of the assembly of Cauchy's stress as defined by Love (1944). Its components are taken positive in compression. In (4), the index j spans the $N(i)$ neighbors of grain i, and the factor $1/2$ avoids twice-counting contacts. The components of the strain tensor $\mathbf{E}$ measure the relative change in length and are taken positive in compression. For example,

$$
E_{11} = (L_1 - l_1)/L_1,
$$

where L_1 and l_1 measure the cell length along the direction 1 before and after the deformation. In elastic systems, increments in stress and strain are related by the fourth-order tensor $\mathbf{C}$,

$$
\Delta\sigma_{rm} = C_{rmij}E_{ij},
\tag{5}
$$

where Einstein's convention is used. In isotropic systems, the tensor $\mathbf{C}$ has two indipendent components, say C_{1111} and C_{1122}. Equivalently, the stress-strain relationship can be expressed in terms of the bulk and shear modulus B and G, as

$$
\begin{aligned}
B &= (C_{1111} + 2C_{1122})/3, \\
G &= (C_{1111} - C_{1122})/2.
\end{aligned}
\tag{6}
$$

3 DEM simulations

3.1 Creation of the initial state

DEM simulations are employed to create four numerical assemblies, labelled by A, B, C and D, each made of 4000 glass spheres confined in a periodic cell. As far as the mechanical properties of glass are concerned, $Y = 70\ GPa$ and $\nu = 0.3$ are its
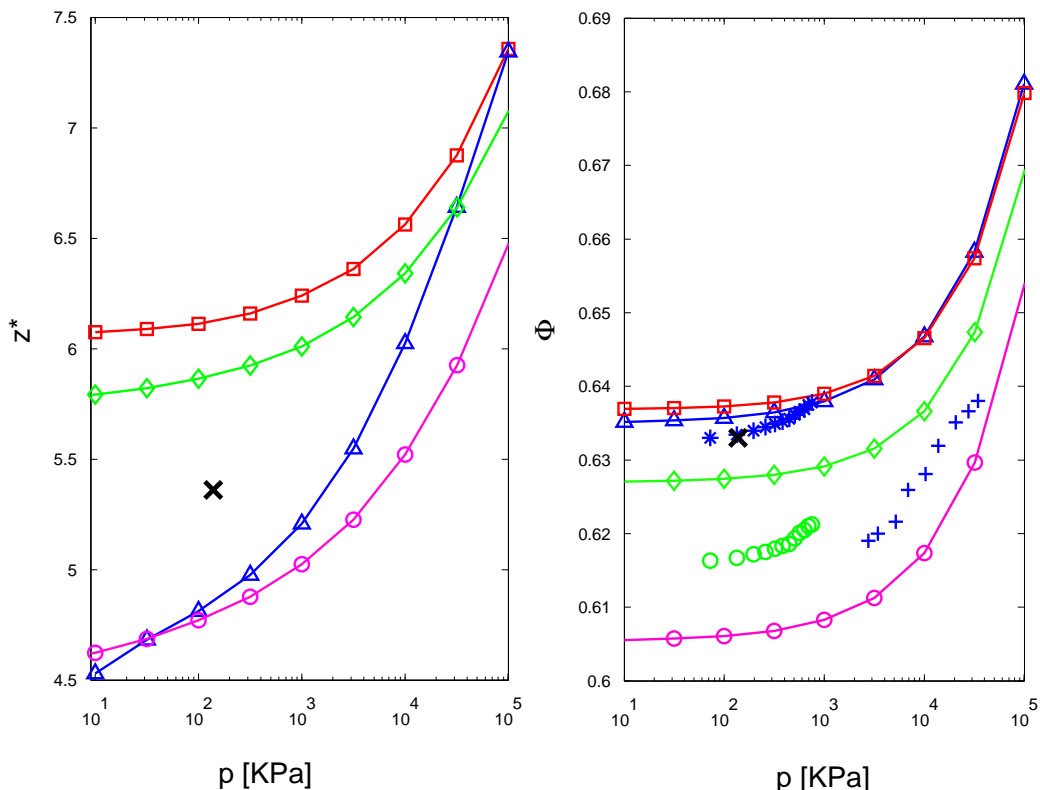
Figure 1: Evolution of coordination number z^* (average number of contacts per active particle) and density Φ with pressure for numerical samples A($\square$), B($\diamond$), C($\triangle$) and D($\bigcirc$). Symbols (*) and (o) are, in turn, for vibrated and lubricated samples in the experiments by Jia and Mills reported in (Agnolin et al., 2005); (+) for the experiments by Domenico (1977); the isolated thick **x** indicates the numerical simulation by Cundall et al. (1989).

Young's and Poisson's modulus, respectively. The evolution of an assembly is studied by integrating in time the equations of motion of the individual grains, which interact through contact forces. Each sample is assembled following a different preparation procedure, and is at equilibrium at the pressure of $10KPa$. The lowest pressure points in Figure 1 give density and coordination number of the initial states. By "equilibrium" it is meant that the resultant force and torque on each grain are smaller than $pD^2/10^4$ and $pD^3/10^4$, respectively. Moreover, the kinetic energy has to be smaller than $pD^3/10^7$, and once all velocities have been set to zero, the kinetic energy must stay null. The initial state of sample A results from the isotropic compression of a frictionless granular gas up to the pressure of $10KPa$, and has coordination number close to 6. Procedure A is a classic in the literature about granular media (Thornton, 2000; Makse et al., 2004), as it is easy to reproduce and gives good agreement with experimental solid fractions. In the case of sample B, the isotropic compression is

7

applied on slightly frictional grains ($\mu = 0.02$), as in an imperfect lubrication. The initial state of sample B is less dense than that of sample A, but still has a large coordination number. The procedure employed to create sample C interprets vibration, which is currently used to compact experimental samples, as a temporary suppression of friction. In this procedure, the coordinates of the grains of the initial state of sample A are first scaled by a factor 1.005. In this way, all contacts are opened. Then, the grains are mixed with random collisions that preserve kinetic energy until they undergo 50 collisions on average. Only at this point is the isotropic compression resumed and continued up to the pressure $P = 10KPa$, with friction $\mu = 0.3$. Sample C is only slightly less dense than A, but has a much lower coordination number, because of friction, and 13% of its grains do not carry any force. These grains are called "rattlers" in the literature. The comparison between density and coordination number of samples A and B on one side and C on the other emphasizes that large densities do not necessarily imply large coordination numbers. Lastly, sample D is the result of the isotropic compression of a frictional gas with friction coefficient $\mu = 0.3$. The initial state of sample D has low density and low coordination number, and 11% of its grains are rattlers.

3.2 Isotropic compression and elastic moduli

From their initial state, the samples are slowly isotropically compressed up to the pressure $p = 10^5 KPa$ via DEM simulations. By 'slow' it is meant that the dimensionless control parameter $I = \dot{E}\sqrt{m/Dp}$ stays smaller than 10^{-4}. In the expression of I, E is the absolute value of the macroscopic deformation. The parameter I has been defined in (da Cruz et al., 2005), and compares the macroscopic deformation rate to the particle-scale time necessary for a grain initially at rest to cover the distance $D/2$ when pushed by a force $F = pD^2$.

At eight intermediate values of pressure the assemblies are allowed to reach equilibrium, and their bulk and shear modulus B and G are measured. B is determined by measuring the macroscopic strain E_{rm} induced by a small isotropic increment in stress

$$\Delta\sigma_{rm} = \Delta p \, \delta_{rm},$$

where δ_{rm} is the identity tensor. Due to (5) and (6),

$$B = \Delta p / 3 E_{ii}.$$

The shear modulus G is determined by measuring the macroscopic strain induced by an incremental stress of the form

$$\Delta\sigma = \Delta q \begin{bmatrix} 1 & 0 & 0 \\ 0 & -1/2 & 0 \\ 0 & 0 & -1/2 \end{bmatrix}, \tag{7}$$

as

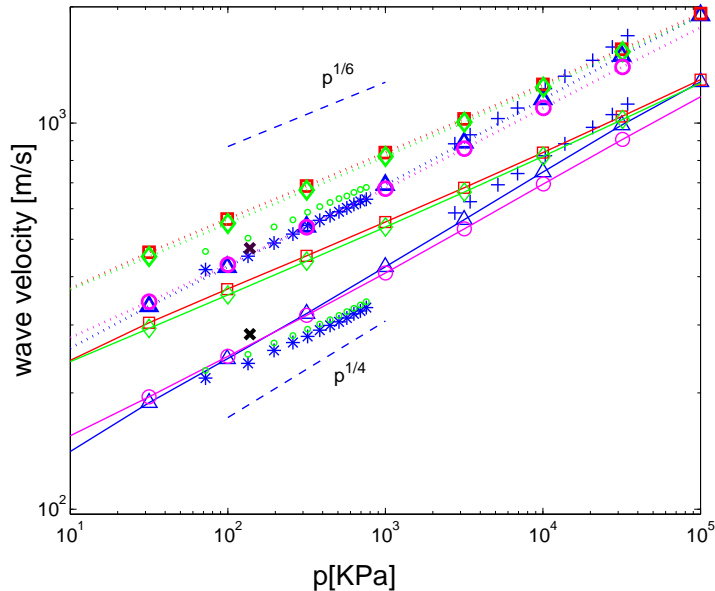$$G = \Delta q / 2 \left(E_{11} - E_{22} \right). \tag{8}$$

8

Figure 2: Wave velocities for numerical samples A($\square$), B($\diamond$), C($\triangle$) and D($\bigcirc$). Dotted and solid lines are used for longitudinal and shear wave velocity v_l and v_s, respectively. Symbols * and $\circ$ are used, in turn, for the experimental results on dry and lubricated grains in Agnolin et al. (2005); + for those in Domenico (1977); the isolated thick x indicates the numerical simulation by Cundall et al. (1989). For each experiment, the upper and lower series measure, in turn, v_l and v_s.

The elastic moduli are plotted in Figure 2 in terms of longitudinal and transversal wave velocities v_L and v_S,

$$
\begin{aligned}
v_L &= \sqrt{(B + 4G/3)/\rho}, \\
v_S &= \sqrt{G/\rho},
\end{aligned}
$$

where ρ is the density of the assembly. The elastic moduli of samples C and D are clearly separated from those of samples A and B, each pair having similar coordination number. Numerical compaction by vibration gives denser but less stiff samples than lubrication, in accordance with experiments, but in contrast with the general belief that the larger the density the stiffer the assembly.

The plot of wave velocities allows comparison with wave propagation experiments. We consider the experiments reported in (Agnolin et al., 2005) and (Domenico, 1977) on samples of glass beads, whose density evolution with pressure is also shown in Figure 1. Only sample C matches the experiments satisfactorily in terms of both stiffness and density, which makes its study relevant. On the contrary, sample A, whose properties are generally referred to in the literature, is too stiff in the range of pressures usual

9

in geotechnical tests. This completes the observations by Makse et al. (2004), who compare sample A only to the large pressure tests of Domenico and conclude that it is representative of real assemblies. In the range of pressure considered by Domenico, the configurations of samples C converge to those of sample A, as the former is derived from the latter. In both experiments and numerical simulations, compaction by vibration gives denser but less stiff samples than lubrication. Also shown in Figures 1 and 2 are density, coordination number and mechanical properties of the numerical sample studied in Cundall et al. (1989). This numerical simulation aims to reproduce the mechanical behavior of a real assembly created by raining spherical beads into a membrane and tamping them. The numerical sample is created by means of an initial almost frictionless compression followed by a series of increasingly frictional expansions and compressions, up to the point where experimental pressure and density are matched. The shear modulus of the numerical sample is 127 MPa, which compares well with the experimental measurement of 161 MPa. Its coordination number is smaller than 6, as in the case of sample C. All these observations emphasize a much stronger dependence of the elastic moduli on coordination number than on density. They also show that some of the numerical samples exhibit properties of experimental ones. A thorough analysis of the resemblance between numerical simulations and experiments requires an extensive study of the internal structure and comparison with the recent experiments reported in Aste et al. (2005). These are deferred to a publication to appear (Agnolin and Roux, 2007), as the present article focuses on the elastic moduli of the numericla samples. In the referred to publication, the reader will also find an accurate discussion of the numerical procedures employed.

3.3   Linear elastic regime

In the previous section, the elastic moduli of the numerical samples have been measured by employing DEM simulations. In order for elasticity to apply, these have to be free from dissipation and quasi-static, while linearity requires that all change in geometry be negligible at the first order. This paragraph identifies the range of deformation inside which such requirements are satisfied, and thus validates the results of the previous section.

Quasi-staticity implies that in the transition between two equilibrium states all dynamic contributions stay negligible. This reduces the forces on the grains to their Hertzian interaction, whose expression can be finally linearized for small enough deformations. An increment $\Delta F_r^{(ij)}$ in the contact force that grain j exerts on grain i can thus be related to the relative displacement $u^{(ij)}$ between the two grains via a normal and a tangential contact stiffness $K_N^{(ij)}$ and $K_T^{(ij)}$. From (1), the normal contact stiffness has the form

$$K_N^{(ij)} = \frac{dF_N}{dh^{(ij)}} = \frac{Y\sqrt{Dh^{(ij)}}}{2(1-\nu^2)},\tag{9}$$

while (2) still holds along the tangential direction. $K_N^{(ij)}$ and $K_T^{(ij)}$ define the contact

stiffness operator

$$K_{ra}^{(ij)} \doteq K_N^{(ij)} n_r^{(ij)} n_a^{(ij)} + K_T^{(ij)} (\delta_{ra} - n_r^{(ij)} n_a^{(ij)}), \tag{10}$$

which makes it possible to write that

$$\Delta F_r^{(ij)} = -K_{ra}^{(ij)} u_a^{(ij)}. \tag{11}$$

The relative displacement $u_a^{(ij)}$ at the contact point between grains i and j is the sum of the contributions $u_a^{E(ij)}$ from the average strain and $\tilde{u}_a^{(ij)}$ from fluctuations. If $\tilde{u}_a^{(i)}$ is the fluctuation of grain i in the center displacement and $\tilde{\omega}_a^{(i)}$ that in the rotation about it, and $\tilde{u}_a^{(j)}$ and $\tilde{\omega}_a^{(j)}$ are the analogous quantities for grain j,

$$u_a^{(ij)} = u_a^{E(ij)} + \tilde{u}_a^{(ij)},$$
$$u_a^{E(ij)} = DE_{am} n_m^{(ij)},$$
$$\tilde{u}_a^{(ij)} = \tilde{u}_a^{(i)} - \tilde{u}_a^{(j)} + \frac{D}{2} \epsilon_{abc} \left[\tilde{\omega}_b^{(i)} + \tilde{\omega}_b^{(j)} \right] n_c^{(ij)}, \tag{12}$$

where ϵ_{abc} is Edington's epsilon. The balance of force and torque on grain i requires that

$$\sum_{j=1}^{N(i)} \Delta F_r^{(ij)} = 0,$$
$$\sum_{j=1}^{N(i)} \epsilon_{abr} n_b^{(ij)} \Delta F_r^{(ij)} = 0, \tag{13}$$

where the index j spans over the $N(i)$ neighbors of i. Lastly, if the increment in stress $\Delta\sigma_{rm}$ applied in the DEM simulation is to balance,

$$-\frac{D}{2V} \sum_{i=1}^{N_{act}} \sum_{j=1}^{N(i)} \Delta F_r^{(ij)} n_m^{(ij)} = \Delta\sigma_{rm}. \tag{14}$$

According to the definition of linearity, the components of the normal contact vector in (13) and (14) are taken to be those found before the increment in stress is applied. Introducing (11) and (12) in the system of (13) and (14) makes it solvable for the 3 non-zero components of the strain and the $6N_{act}$ grain fluctuations. The deformation range inside which the results coincide with those of the DEM simulations strongly depends on coordination number and increases with pressure. For confining pressure between $10KPa$ and $1MPa$, it varies between 10^{-6} and 10^{-5} for sample C, and between 10^{-5} and 10^{-4} for sample A. For larger deformations grain rearrangement cannot be neglected. The fluctuations that result from these calculations will be analysed in section 5.
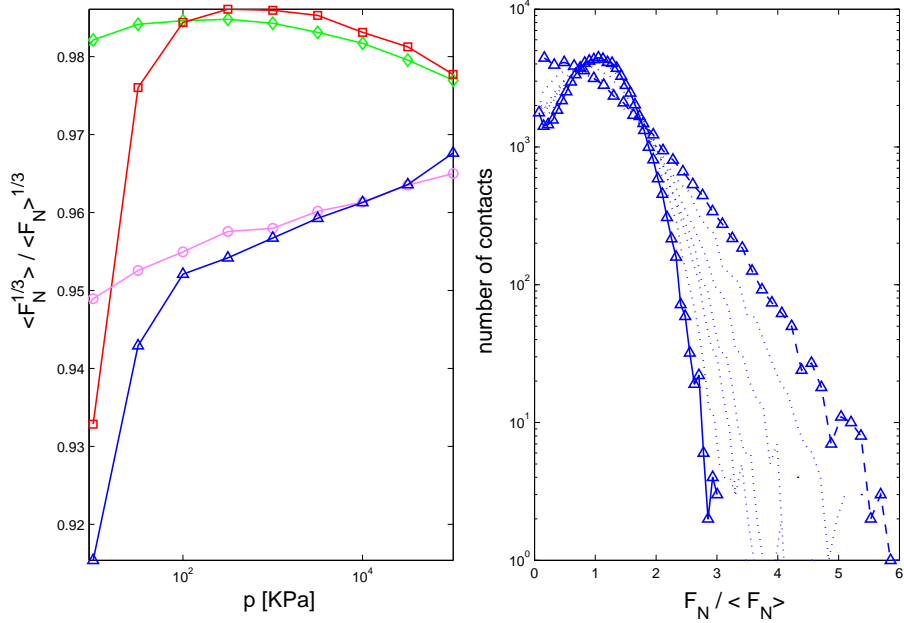
Figure 3: Left-hand side: evolution of the quantity $\langle F^{1/3}\rangle/\langle F\rangle^{1/3}$ for samples A($\square$), B($\diamond$), C($\triangle$) and D($\bigcirc$). Right-hand side: evolution of the normal contact force distribution for sample C; the dashed and solid line reperesent, in turn, the distribution at $p = 10$ and $10^5 KPa$; dotted lines are used at intermediate pressures.

4 Average strain assumption

In the attempt to predict the elastic moduli, the easiest scenario possible is that of relative displacements between contacting grains driven by the average strain. The corresponding incremental overlap $h^{E(ij)}$ and tangential relative displacement $s_a^{E(ij)}$ would be

$$
\begin{aligned}
h^{E(ij)} &= DE_{lm}n_l^{(ij)}n_m^{(ij)}, \\
s_a^{E(ij)} &= DE_{am}n_m^{(ij)} - h^{E(ij)}n_a^{(ij)},
\end{aligned}
\tag{15}
$$

which depend on the contact orientation alone. Expressions (11) and (15) are introduced in (4), and the discrete expression for the stress is transformed into an integral over the solid angle. To this aim, an isotropic probability distribution function $f(\psi) = z/4\pi$ is employed, which is defined in such a way that $f(\psi)\,d\psi$ is the number of contacts in the element of solid angle $d\psi$. As a result,

$$
\Delta\sigma_{rm} = -\frac{D^2 N_{act}}{2V}\langle K_{ra}\rangle \int_0^{4\pi} E_{ab}n_b n_m f(\psi)\,d\psi,
\tag{16}
$$

12

where K_{ra} is the average contact stiffness. From (2) and (9),

$$
\begin{aligned}
< K_N > &= \left[\frac{3DY^2}{8\left(1-\nu^2\right)^2}\right]^{1/3} < F_N^{1/3} >, \\
< K_T > &= \frac{2(1-\nu)}{2-\nu} < K_N >,
\end{aligned}
\tag{17}
$$

which with (5) and (6) give the estimates

$$
\begin{aligned}
B^E &= \frac{1}{2}\left[\frac{z\Phi Y}{3\pi}\right]^{2/3} P^{1/3}\frac{< F_N^{1/3} >}{< F_N >^{1/3}}, \\
G^E &= \frac{6 + 9\langle K_T\rangle/\langle K_N\rangle}{10}B^E.
\end{aligned}
\tag{18}
$$

For contacts between glass spheres, $\langle K_T\rangle/\langle K_N\rangle = 0.823$. Expressions (18) account for the width of the normal force distribution, whose evolution with pressure for sample C is shown in Figure 3. If this is assumed uniform, the estimates reduce to those of Walton (1987):

$$
\begin{aligned}
B^{EW} &= \frac{1}{2}\left[\frac{z\Phi Y}{3\pi}\right]^{2/3} P^{1/3}, \\
G^{EW} &= \frac{6 + 9\langle K_T\rangle/\langle K_N\rangle}{10}B^{EW}.
\end{aligned}
\tag{19}
$$

Figure 3 shows that the difference between estimates (18) and (19) is rather small, and larger for samples A and C. The ratio of B^E and G^E to the effective moduli is plotted in Figure 4, where it is observed that the prediction of the bulk modulus is reliable. On the contrary, that of the shear modulus performs poorly, and improvement can be obtained only at the expenses of incorporating the displacement fluctuations into the modelling.

5   Fluctuations

We study the displacement fluctuations that arise when the shear stress (7) is applied, and interpret the role of the various kinematic ingredients. Coherently with the constitutive law for the contact force (11), the fluctuations are analyzed in terms of the relative displacement they induce at the contact points. This is denoted by $\tilde{u}_a^{(ij)}$ in (12). Its normal and tangential components $\tilde{h}^{(ij)}$ and $\tilde{s}_a^{(ij)}$ are

$$
\begin{aligned}
\tilde{h}^{(ij)} &= \tilde{u}_l^{(ij)}n_l^{(ij)}, \\
\tilde{s}_a^{(ij)} &= \tilde{u}_a^{(ij)} - \tilde{h}^{(ij)}n_a^{(ij)}.
\end{aligned}
\tag{20}
$$

In the tangent plane, $\tilde{s}_a^{(ij)}$ is still the sum of $\tilde{w}^{(ij)}t_a^{E(ij)}$ and $\tilde{z}_a^{(ij)}$, in turn aligned with and perpendicular to the tangential displacement $s_a^{E(ij)}$ induced by the average strain.
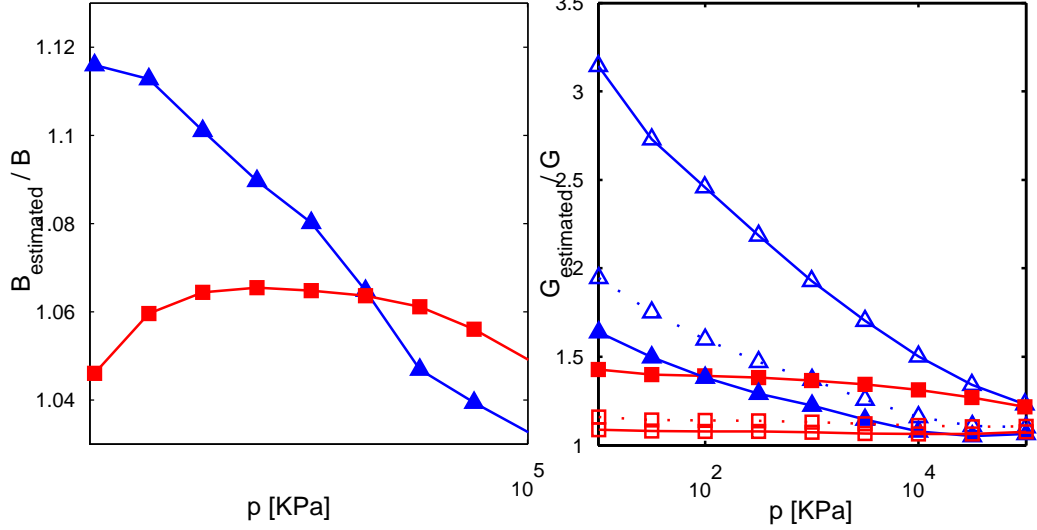
13

Figure 4: Ratio of estimated to measured bulk (left) and shear (right) modulus for sample A($\square$) and C($\triangle$). Filled symbols indicate the results of the average strain assumption; empty symbols indicate the estimate of the shear modulus in the 1FP (dashed line) and the FP approach (solid line).

If $t_a^{E(ij)}$ is defined as the unit vector aligned with $s_a^{E(ij)}$,

$$
\begin{aligned}
t_a^{E(ij)} &\doteq s_a^{E(ij)}/|s^{E(ij)}|, \\
\tilde{w}^{(ij)} &= \widetilde{s}_l^{(ij)} t_l^{E(ij)}, \\
\tilde{z}_a^{(ij)} &= \tilde{s}_a^{(ij)} - \tilde{w}^{(ij)} t_a^{E(ij)},
\end{aligned}
\tag{21}
$$

with $t_a^{E(ij)} \tilde{z}_a^{(ij)} = 0$. Further distinction is made in $\tilde{w}^{(ij)}$ between the contributions $\tilde{w}^{u(ij)}$ from the displacement of the centers and $\tilde{w}^{\omega(ij)}$ from rotations, i.e.

$$
\begin{aligned}
\tilde{w}^{u(ij)} &= \left[\tilde{u}_l^{(i)} - \tilde{u}_l^{(j)}\right] t_l^{E(ij)}, \\
\tilde{w}^{\omega(ij)} &= \frac{D}{2}\epsilon_{lbc}\left[\tilde{\omega}_b^{(i)} + \tilde{\omega}_b^{(j)}\right] n_c^{(ij)} t_l^{E(ij)}, \\
\tilde{w}^{(ij)} &= \tilde{w}^{u(ij)} + \tilde{w}^{\omega(ij)}.
\end{aligned}
\tag{22}
$$

We organize the contacts in sets depending on the polar angle θ with respect to the major principal stress, as axial symmetry in the applied stress and isotropy in the contact orientation make the displacement fluctuations depend on it. We denote by $S_{\overline{\theta}}$ the set of polar angle $\overline{\theta}$, and consider *equally oriented* all contacts that belong to it.
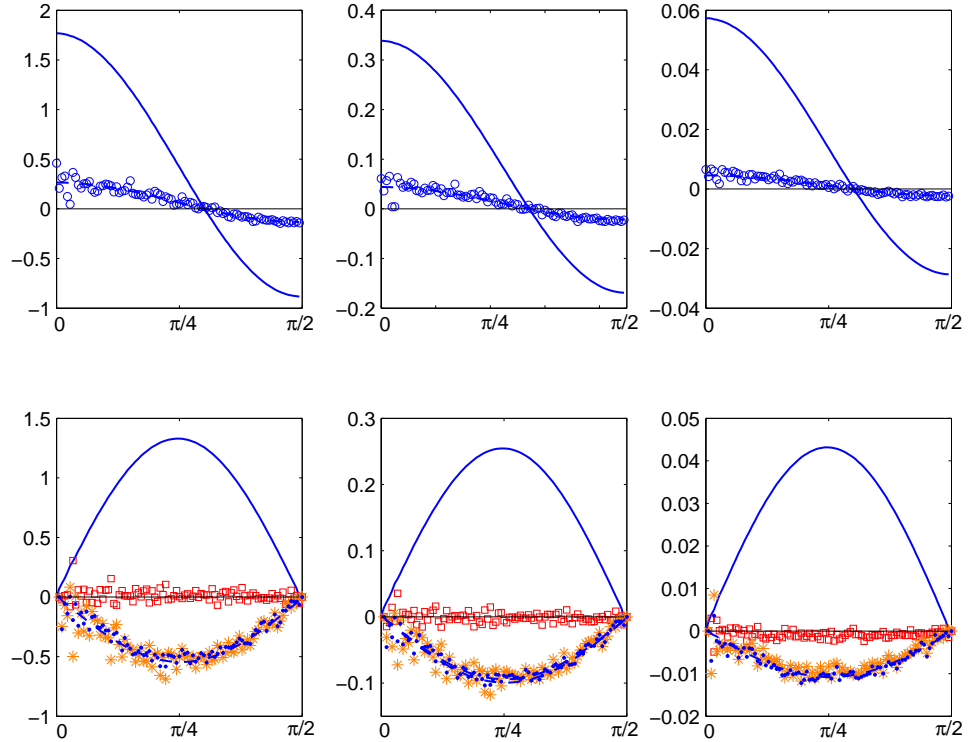
14

Figure 5: Normal (first row) and tangential (second row) contact displacements for sample A, averaged over equally oriented contacts, at $p = 10KPa$ (left), $p = 10^3 KPa$ (center) and $p = 10^5 KPa$. The results are in diameter units, multiplied by 10^4. Solid lines indicate the average strain contribution; symbols: $\bullet = <\tilde{w}>$; $* = <\tilde{w}^\omega>$; $\square = <\tilde{w}^u>$.

Firstly, in Figures 5 and 6 we plot the fluctuations averaged over each set, for sample A and C, respectively, with the polar angle made vary between 0 and 90 degrees. Sample A is also representative of the behavior of sample B, which has a similar coordination number; in the same way, sample C is also representative of sample D. That is, the displacement fluctuations chiefly depend on coordination number. Set by set, the $\tilde{z}_a$'s are zero on average. Open and filled dots represent, in turn, the average of $\tilde{h}^{(ij)}$ and $\tilde{w}^{(ij)}$, which we denote by $\langle \tilde{h} \rangle_\theta$ and $\langle \tilde{w} \rangle_\theta$. These are found to be proportional to the displacement induced by the average strain and aligned with them. As a result, it is possible to write that

$$
\begin{aligned}
\langle \tilde{h} \rangle_\theta &= \alpha_N h^{E(ij)}, \\
\langle \widetilde{w} \rangle_\theta &= \alpha_T s_a^{E(ij)} t_a^{E(ij)},
\end{aligned}
\tag{23}
$$

with α_N and α_T the proportionality factors. α_N and α_T are negative, because the fluctuations counteract the average strain. Their value is reported in Table 1, which shows that the tangential fluctuations are significantly more effective than the radial
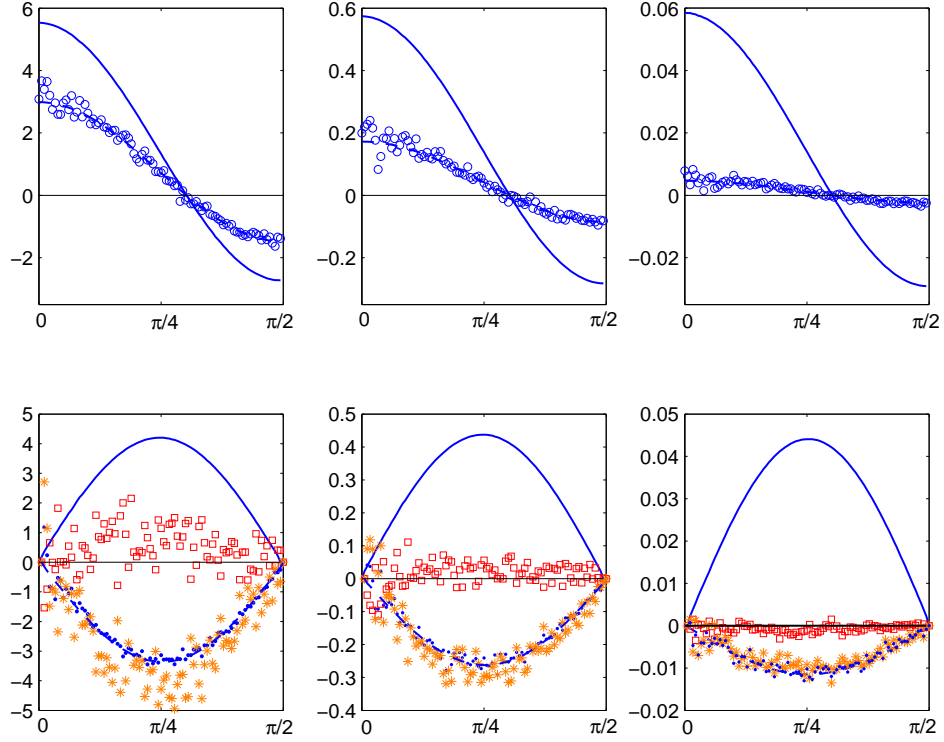
15

Figure 6: Normal (first row) and tangential (second row) contact displacements for sample C. Same symbols as in Figure 5.

ones in relaxing the system. Contact by contact, $\tilde{h}^{(ij)}$ and $\widetilde{w}^{(ij)}$ may significantly differ from their average $\langle \tilde{h} \rangle_\theta$ and $\langle \widetilde{w} \rangle_\theta$. If the difference from the average is called "residual" and labelled by a superscript R, then

$$
\begin{aligned}
\tilde{h}^{(ij)} &= \alpha_N h^{E(ij)} + h^{R(ij)}, \\
\widetilde{w}^{(ij)} &= \alpha_T s_a^{E(ij)} t_a^{E(ij)} + w_a^{R(ij)} t_a^{E(ij)}.
\end{aligned}
\tag{24}
$$

As α_N and α_T are independent of the polar angle, $\langle \tilde{h} \rangle_\theta$ and $\langle \widetilde{w} \rangle_\theta$ are determined by the average structure of the assembly.

Secondly, we want to understand how the displacement fluctuations determine the macroscopic behavior of the assemblies. As they depend on the contact overlap, both the normal and the tangential contact stiffness fluctuate about an average, and one can write that

$$
\begin{aligned}
K_N^{(ij)} &= <K_N> + \tilde{K}_N^{(ij)}, \\
K_T^{(ij)} &= <K_T> + \tilde{K}_T^{(ij)}.
\end{aligned}
\tag{25}
$$

Once (11), (12), (20), (21), (24) and (25) have been inserted in (4), and sums over

16

Sample A				Sample B			
p[KPa]	α_N	α_T	α_T^ω	p[KPa]	α_N	α_T	α_T^ω
10	-0.16	-0.41	-0.46	10	-0.16	-0.46	-0.48
$10\sqrt{10}$	-0.14	-0.42	-0.43	$10\sqrt{10}$	-0.16	-0.45	-0.47
10^2	-0.14	-0.39	-0.40	10^2	-0.15	-0.44	-0.46
$10^2\sqrt{10}$	-0.14	-0.4	-0.40	$10^2\sqrt{10}$	-0.15	-0.43	-0.44
10^3	-0.13	-0.37	-0.38	10^3	-0.15	-0.41	-0.43
$10^3\sqrt{10}$	-0.13	-0.36	-0.36	$10^3\sqrt{10}$	-0.14	-0.39	-0.41
10^4	-0.10	-0.33	-0.33	10^4	-0.13	-0.36	-0.36
$10^4\sqrt{10}$	-0.09	-0.30	-0.23	$10^4\sqrt{10}$	-0.10	-0.33	-0.33
10^5	-0.07	-0.25	-0.31	10^5	-0.08	-0.28	-0.26
Sample C				Sample D			
10	-0.54	-0.80	-1.04	10	-0.49	-0.78	-0.96
$10\sqrt{10}$	-0.48	-0.76	-0.96	$10\sqrt{10}$	-0.48	-0.77	-0.91
10^2	-0.44	-0.73	-0.90	10^2	-0.45	-0.74	-0.89
$10^2\sqrt{10}$	-0.36	-0.68	-0.81	$10^2\sqrt{10}$	-0.40	-0.71	-0.82
10^3	-0.30	-0.60	-0.71	10^3	-0.34	-0.67	-0.77
$10^3\sqrt{10}$	-0.24	-0.53	-0.60	$10^3\sqrt{10}$	-0.29	-0.61	-0.69
10^4	-0.18	-0.45	-0.49	10^4	-0.24	-0.54	-0.59
$10^4\sqrt{10}$	-0.13	-0.35	-0.37	$10^4\sqrt{10}$	-0.19	-0.46	-0.48
10^5	-0.09	-0.26	-0.27	10^5	-0.15	-0.37	-0.37

Table 1: Contribution from the structural fluctuations to the stress for samples A, B, C, D.

grains have been transformed into sums over contacts spanning the sets $S(\theta)$, one obtains

$$
\begin{aligned}
\Delta\sigma_{rm}\frac{V}{D} &= \sum_\theta \sum_{(ij)\in S_\theta} \left[<K_N> +\tilde{K}_N^{(ij)} \right] \left[(1+\alpha_N)\,h^{E(ij)} + h^{R(ij)} \right] n_r^{(ij)} n_m^{(ij)} \\
&+ \sum_\theta \sum_{(ij)\in S_\theta} \left[<K_T> +\tilde{K}_T^{(ij)} \right] \left[\delta_{rl} - n_r^{(ij)} n_l^{(ij)} \right] \\
&\qquad\times \left[(1+\alpha_T)\,s_l^{E(ij)} + w^{R(ij)} t_l^{E(ij)} + \tilde{z}_l^{(ij)} \right] n_m^{(ij)}.
\end{aligned}
$$

With respect to (4), the factor $1/2$ has disappeared, as double counting does not occur when the indexes are made vary over the contacts. Due to the definition of fluctuations, products of fluctuations in the contact stiffness, the residuals or the $\tilde{z}_l$'s times the average stiffness, the $h^{E(ij)}$ or the $s_l^{E(ij)}$'s give null terms. In what remains, products of fluctuations give contributions whose ratio to the total stress ranges between 10^{-3} and 10^{-7}, and which can thus be neglected. As a consequence,

$$
\begin{aligned}
\Delta\sigma_{lm}\frac{V}{D} &\simeq <K_N>(1+\alpha_N)\sum_\theta \sum_{(ij)\in S_\theta} h^{E(ij)} n_l^{(ij)} n_m^{(ij)} \\
&+ <K_T>(1+\alpha_T)\sum_\theta \sum_{(ij)\in S_\theta} s_l^{E(ij)} n_m^{(ij)}.
\end{aligned}
\tag{26}
$$

Expression (26) makes it explicit that the average structure is defined by the average contact stiffness and the average contact distribution. Local deviations from the average structure give rise to the residuals and the $\tilde{z}$'s, which disappear at the macroscopic scale. However, their numerical value is comparable to that of the average fluctuations, as Figure 7 proves. In this figure, the absolute value of the residuals, averaged over equally oriented contacts, is inferred by comparing the absolute value of normal and tangential fluctuations, averaged over the contact sets, with the absolute value
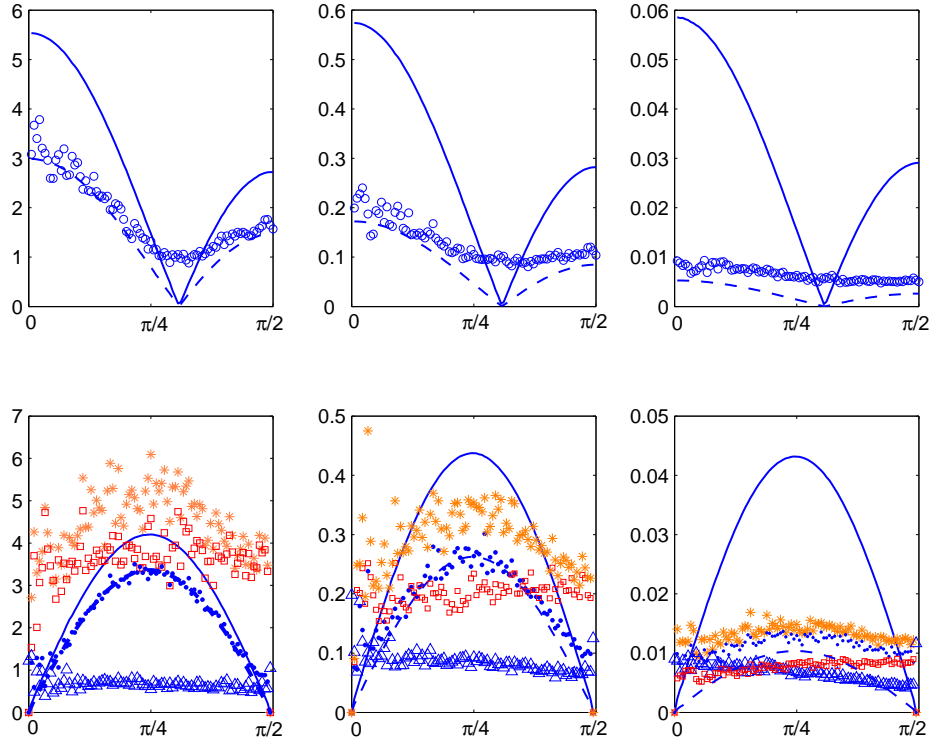
17

Figure 7: Modulus of normal (first row) and tangential (second row) contact displacements averaged over equally oriented contacts and multiplied by 10^4. Same symbols as in Figure 5.

of the average. All quantities decrease with increasing coordination number, as the forces induced by the average strain balance more and more easily, but the residuals, especially in the tangent plane, and the $\tilde{z}$'s decrease more slowly than the average fluctuations. This means that the issue of local equilibrium is less sensitive than that of the average structure to coordination number.

As in (16), (26) can be transformed into an integral over the solid angle. As a result,

$$ G = \frac{1}{10} \left[6 \left(1 + \alpha_N \right) + 9 \left(1 + \alpha_T \right) \frac{< K_T >}{< K_N >} \right] B^E, \tag{27} $$

which states that the prediction of the shear modulus requires that of α_N and α_T.

Tangential fluctuations are contributed by both center displacements and rotations. The average over the contact sets of the $\widetilde{w}^{\omega(ij)}$ and $\widetilde{w}^{u(ij)}$, introduced in (22), is also determined, and reported in Figures 5 and 6. This time, significant deviations from the proportionality to $s_a^{E(ij)} t_a^{E(ij)}$ are observed, and especially the $\widetilde{w}^{u(ij)}$'s distribute rather isotropically. In Agnolin and Kruyt (2006), a strict proportionality is still observed in two-dimensional random assemblies of polydisperse disks with identical contact stiffness. Therefore, the poor correlation found for spheres is the specific
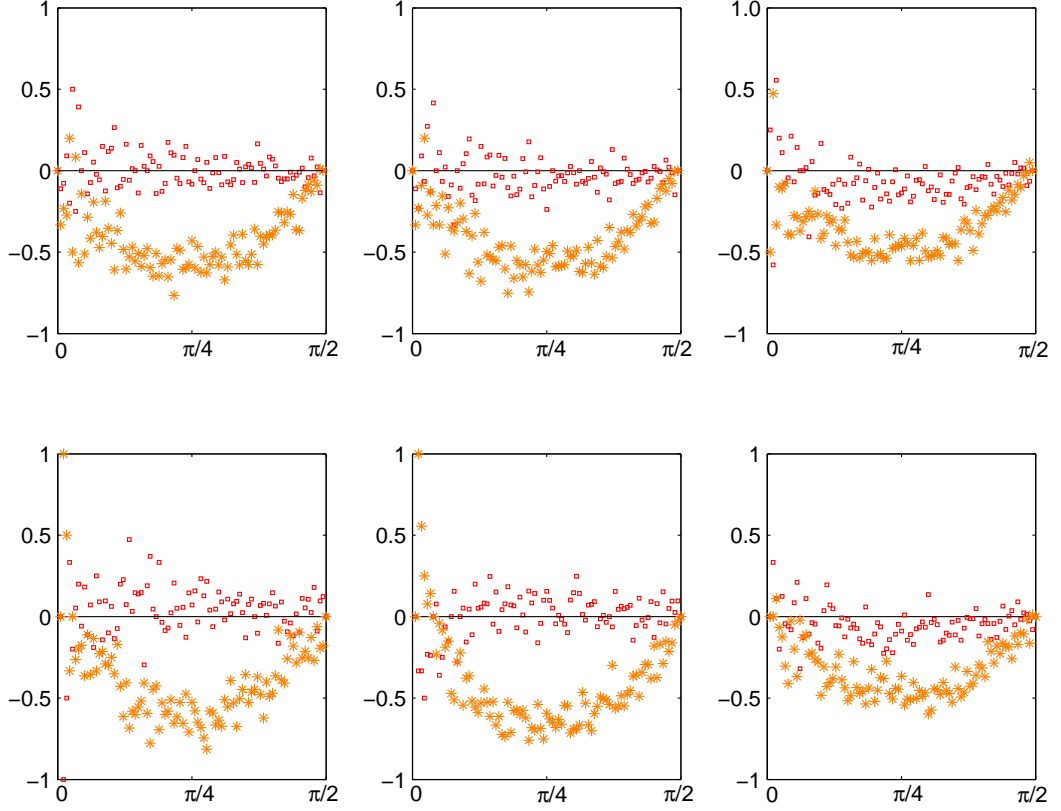
Figure 8: Sign of $\tilde{w}^u$($\square$) and ($\tilde{w}^\omega$)(*) over equally oriented contacts for sample A(first row) and C (second row), at pressure $p = 10$(left), 10^3(center) and $10^5 KPa$(right). A positive (negative) value means the dominance of the positive (negative) sign; the numerical value gives the fraction of contacts that sign prevails by.

signature of inhomogeneity in the contact stiffness. A closer insight into the role of center displacements and rotations is given by averaging $sign\,(\tilde{w}^u)$ and $sign\,(\tilde{w}^\omega)$ over the sets $S(\theta)$. As a definition,

$$
\begin{aligned}
\langle sign\,(\tilde{w}^u)\rangle_\theta &= \sum_{ij\in S(\theta)} \frac{sign\,(\tilde{w}^u)}{N(S_\theta)} = \frac{N^+\,(\tilde{w}^u) - N^-\,(\tilde{w}^u)}{N(S_\theta)}, \\
\langle sign\,(\tilde{w}^\omega)\rangle_\theta &= \sum_{ij\in S(\theta)} \frac{sign\,(\tilde{w}^\omega)}{N(S_\theta)} = \frac{N^+\,(\tilde{w}^\omega) - N^-\,(\tilde{w}^\omega)}{N(S_\theta)},
\end{aligned}
$$

where $N(S_\theta)$ is the number of contacts in the set S_θ, and $N^+(\;)$ and $N^-(\;)$ give the number of contacts at which the bracketed quantity is, in turn, positive and negative. A (positive) negative result means that at the chosen polar angle the fluctuations mainly (do not) counteract the displacements induced by the average strain, while the

numerical value specifies the percent of contacts the dominant sign prevails by. Figure 8, which refers to sample C, shows that rotations mainly oppose the average strain, the more efficiently the larger the displacements induced by the average strain. Exceptions are the closest orientations to the main compression. However, the corresponding contact sets are not statistically representative, because of the low number of contacts they gather due to isotropy in the distribution of the contact orientation. As far as the center displacements are concerned, these do not counteract the average strain, especially at small coordination numbers. From (26), one can also say that

$$
\begin{aligned}
\alpha_N &= \Delta\sigma_{lm}(\widetilde{h})/\Delta\sigma_{lm}(h^E), \\
\alpha_T &= \Delta\sigma_{lm}(\tilde{w})/\Delta\sigma_{lm}(s^E),
\end{aligned}
\tag{28}
$$

where brackets include the kinematic term whose contribution to the stress is considered. By analogy with (28), we introduce the numerical factors α_T^ω and α_T^u, namely

$$
\begin{aligned}
\alpha_T^\omega &\doteq \Delta\sigma_{lm}(\widetilde{w}^\omega)/\Delta\sigma_{lm}(s^E), \\
\alpha_T^u &\doteq \Delta\sigma_{lm}(\widetilde{w}^u)/\Delta\sigma_{lm}(s^E),
\end{aligned}
\tag{29}
$$

which allow to measure the contribution to the macroscopic behavior from rotations and center displacements. α_T^ω is also reported in Table 1, averaged over the directions 11, 22 and 33, while α_T^u can be inferred, as $\alpha_T^u = \alpha_T - \alpha_T^\omega$. The contribution from the center displacements is much smaller than that due to rotations. Moreover, the relaxation induced along the tangential direction comes entirely from rotations, with the exception of sample A at the pressure of $10^4\sqrt{10}KPa$ and sample B at the pressure of $10^5\sqrt{10}KPa$.

6   Predictions

Reliable estimates of the shear modulus need to incorporate displacement fluctuations compatible with (23). This is the case in the 1-fluctuating-particle approach (1FP) and in the Pair-Fluctuation (PF) approach, both based on the balance of force and torque on a small-sized subassembly. In this section, the two methods are briefly recalled, numerically emplyed and compared.

The 1-fluctuating-particle approach (1FP) is put forward in Kruyt and Rothenburg (2002) to numerically predict the elastic moduli of two-dimensional assemblies of non-rotating frictional disks. In this approach, the balance of force and moment is solved grain by grain in the assembly. In more detail, the chosen grain alone, say i, is allowed to fluctuate, while its neighbors are compelled to move in accordance with the average strain. As a result, the relative displacement $u_t^{(ia)}$ differs from (12), as

$$
u_t^{(ia)} = DE_{tm}n_m^{(ia)} + \tilde{u}_t^{(i)} + \frac{D}{2}\epsilon_{tbc}\tilde{\omega}_b^{(i)}n_c^{(ia)},
\tag{30}
$$

and the equilibrium equations for the chosen grain, i.e.

$$\sum_{a=1}^{N(i)} \left[\left(K_N^{(ia)} - K_T^{(ia)} \right) n_r^{(ia)} n_t^{(ia)} + K_T^{(ia)} \delta_{rt} \right] u_t^{(ia)} = 0,$$

$$\sum_{a=1}^{N(i)} \epsilon_{vgr} n_g^{(ia)} \left[\left(K_N^{(ia)} - K_T^{(ia)} \right) n_r^{(ia)} n_t^{(ia)} + K_T^{(ia)} \delta_{rt} \right] u_t^{(ia)} = 0, \qquad (31)$$

can be solved for its fluctuations if the average strain is considered known. The displacement at the contact point between interacting grains, say i and j, is conveniently expressed using the notation

$$\begin{aligned} \tilde{u}_r^{(i)} - \tilde{u}_r^{(j)} &= \beta_{rs}^{(ij)} e_s, \\ \tilde{\omega}_r^{(i)} + \tilde{\omega}_r^{(j)} &= \gamma_{rs}^{(ij)} e_s. \end{aligned} \qquad (32)$$

In (32), the vector $\mathbf{e}$ has components

$$e_1 = E_{11}, \; e_2 = E_{22}, \; e_3 = E_{33},$$

and $\beta_{rs}^{(ij)}$ and $\gamma_{rs}^{(ij)}$, which describe the stiffness and geometry of their neighborhood, are inferred from the components of the matrices associated with the two problem of equilibrium (31) for grain i and j. The contact radial shortening $\tilde{h}^{(ij)}$ and the tangential relative displacement $\tilde{\mathbf{s}}^{(ij)}$ that correspond to (32) are

$$\begin{aligned} \tilde{h}^{(ij)} &= \beta_{rm}^{(ij)} e_m n_r^{(ij)}, \\ \tilde{s}_r^{(ij)} &= \beta_{sm}^{(ij)} e_m \left(\delta_{sr} - n_s^{(ij)} n_r^{(ij)} \right) + \frac{D}{2} \epsilon_{rbc} \gamma_{bm}^{(ij)} e_m n_c^{(ij)}. \end{aligned} \qquad (33)$$

On the base of (6) and (5), the contributions $\widetilde{C}_{1111}$ and $\tilde{C}_{1122}$ from the fluctuation of the pairs to the forth order tensor and $\tilde{G}$ to the shear modulus are

$$\begin{aligned} \tilde{C}_{1111} &= \frac{D}{V} \sum_{(ij)=1}^{C} \left[\left(K_N^{(ij)} - K_T^{(ij)} \right) \beta_{r1}^{(ij)} n_r^{(ij)} n_1^{(ij)} \right. \\ &\qquad \left. + K_T^{(ij)} \left(\beta_{11}^{(ij)} + \frac{D}{2} \epsilon_{1bc} \gamma_{b1}^{(ij)} n_c^{(ij)} \right) \right] n_1^{(ij)}, \\ \tilde{C}_{1122} &= \frac{D}{V} \sum_{(ij)=1}^{C} \left[\left(K_N^{(ij)} - K_T^{(ij)} \right) \beta_{r2}^{(ij)} n_r^{(ij)} n_1^{(ij)} \right. \\ &\qquad \left. + K_T^{(ij)} \left(\beta_{12}^{(ij)} + \frac{D}{2} \epsilon_{1bc} \gamma_{b2}^{(ij)} n_c^{(ij)} \right) \right] n_1^{(ij)}, \\ \tilde{G} &= (\tilde{C}_{1111} - \tilde{C}_{1122})/2, \end{aligned} \qquad (34)$$

where the sums are carried out over the contacts in the assembly.

The pair fluctuation model (PF) is employed in Agnolin et al. (2005a) and Jenkins et al. (2005) to analytically predict the shear modulus of, in turn, two-dimensional
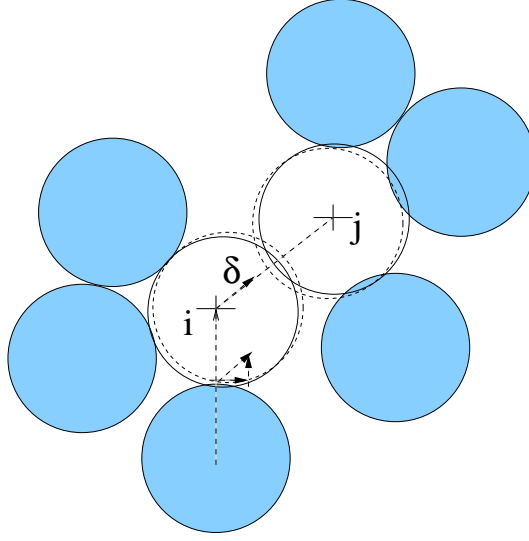
Figure 9: A pair of contacting grains ij with their neighborhood in the PF approach. The pair alone is allowed to fluctuate, while the grains in contact with them are compelled to move in accordance with the average strain. A radial relative displacement δ of the pair induces forces on the neighbors that have non-zero normal and tangential component.

systems of frictional and frictionless disks and of three-dimensional assemblies of frictionless spheres. In this method, the balance of force and torque is solved pair by pair of contacting grains in the assembly. The pair alone is allowed to fluctuate, while its neighborhood is compelled to move in accordance with the average strain, as shown in Figure 9. If i and j are the indexes of the grains of the chosen pair, their relative displacement $u_t^{(ij)}$ is still given by (12), while (30) holds whenever a neighbor of i different from j is considered, and

$$u_t^{(jb)} = DE_{tm}n_m^{(jb)} + \tilde{u}_t^{(j)} + \frac{D}{2}\epsilon_{tbc}\tilde{\omega}_b^{(j)}n_c^{(jb)} \tag{35}$$

is employed when $b \neq i$. With the average strain assigned, the system consisting of the equilibrium equations (31) for grains i and

$$\sum_{b=1}^{N(j)} \left[\left(K_N^{(jb)} - K_T^{(jb)}\right) n_r^{(jb)} n_t^{(jb)} + K_T^{(jb)}\delta_{rt} \right] u_t^{(jb)} = 0,$$

$$\sum_{b=1}^{N(j)} \epsilon_{vgr} n_g^{(jb)} \left[\left(K_N^{(jb)} - K_T^{(jb)}\right) n_r^{(jb)} n_t^{(jb)} + K_T^{(jb)}\delta_{rt} \right] u_t^{(jb)} = 0 \tag{36}$$

for grain j can be solved for the fluctuations of the pair if the average strain is considered known. Expressions (33) and (34) can still be employed to express the relative

22

displacement and the contribution from the pair to the elastic moduli, but this time $\beta_{rs}^{(ij)}$ and $\gamma_{rs}^{(ij)}$ are inferred from the components of the solving matrix associated with the problem of equilibrium of the pair. It is finally noticed that the fluctuations of the individual particles are not unique in the PF method, as each force-carrying grain belongs to more than one pair.

The relative displacements induced by the estimated fluctuations are averaged over equally oriented contacts. Due to the small size of the representative domains, such averages are not nicely proportional anymore to the relative displacements induced by the average strain, especially in the tangential plane. The values of α_N and α_T, which measure the contribution from the fluctuations to the macroscopic stress, are thus determined using (28), and plotted in Figure 10 for samples A and C. The corresponding 1FP and PF estimates of the shear modulus are plotted in Figure 4 in terms of their ratio to the effective value. The results bound the performance that could be achieved by the corresponding analytical solutions, and emphasize a remarkable improvement with respect to the average strain assumption, especially for sample A. In the case of sample C, in the worst case the overestimate is reduced from 3.3 to about 1.5: further improvement would require to incorporate, at least, the fluctuations of the first neighbors. The results allow to conclude that the fluctuations which most affect the macroscopic behavior do correlate within short distance, in accordance with Gaspar and Koenders (2001) and Agnolin and Kruyt (2006), the more the larger the coordination number. In contrast with the results obtained by Agnolin and Kruyt (2006) in two dimensions, the tangential fluctuations are better predicted than the radial ones.

6.1   1FP vs PF

The PF approach gives worse estimates than the 1FP method, even though it relaxes more degrees of freedom. In order to get a better insight into this finding, we focus on two contacting grains, say i and j, and compare the equilibrium equations that result for the pair from the two approaches. Three quantities describe the stiffness of the neighborhood of grain i in (31), namely

$$
\begin{aligned}
I_{rt}^{(ij)} &\doteq \sum_{a=1}^{N(i)} K_{rt}^{(ia)}, \\
J_{rts}^{(ij)} &\doteq \sum_{a=1}^{N(i)} n_r^{(ia)} K_{ts}^{(ia)}, \\
P_{rtsg}^{(ij)} &\doteq \sum_{a=1}^{N(i)} n_r^{(ia)} K_{ts}^{(ia)} n_g^{(ia)},
\end{aligned}
\tag{37}
$$

which we have labelled by (ij) because of our focus on the pair. Analogous quantities, say $I_{rt}^{(ji)}$, $J_{rts}^{(ji)}$ and $P_{rtsg}^{(ji)}$, stem from the equilibrium of grain j. Sums like these, whose largest order depends on the size of the subsystem on which equilibrium is

enforced, were first studied by Koenders (1987), who called them "structural sums". If the equations of balance of the force and torque are, in turn, subtracted from and summed to each other, one obtains in the 1FP case:

$$
\begin{aligned}
& 2 \left\{ - \left[I_{rt}^{(ij)} + I_{rt}^{(ji)} \right] \left(\tilde{u}_t^{(i)} - \tilde{u}_t^{(j)} \right) - \left[I_{rt}^{(ij)} - I_{rt}^{(ji)} \right] \left(\tilde{u}_t^{(i)} + \tilde{u}_t^{(j)} \right) \right\} \\
+ \; & \epsilon_{sbc} D \left\{ \left[J_{brs}^{(ij)} - J_{brs}^{(ji)} \right] \left(\tilde{\omega}_c^{(i)} + \tilde{\omega}_c^{(j)} \right) + \epsilon_{sbc} D \left[J_{brs}^{(ij)} + J_{brs}^{(ji)} \right] \left(\tilde{\omega}_c^{(i)} - \tilde{\omega}_c^{(j)} \right) \right\} \\
= \; & -4D \left[J_{crs}^{(ij)} - J_{crs}^{(ji)} \right] E_{sc}, \\
& 2\epsilon_{sbc} \left\{ - \left[J_{bct}^{(ij)} - J_{bct}^{(ji)} \right] \left(\tilde{u}_t^{(i)} - \tilde{u}_t^{(j)} \right) - \left[J_{bct}^{(ij)} + J_{bct}^{(ji)} \right] \left(\tilde{u}_t^{(i)} + \tilde{u}_t^{(j)} \right) \right\} \\
+ \; & \epsilon_{sbv} \epsilon_{drc} D \left\{ \left[P_{bvdr}^{(ij)} + P_{bvdr}^{(ji)} \right] \left(\tilde{\omega}_c^{(i)} + \tilde{\omega}_c^{(j)} \right) + \left[P_{bvdr}^{(ij)} - P_{bvdr}^{(ji)} \right] \left(\tilde{\omega}_c^{(i)} - \tilde{\omega}_c^{(j)} \right) \right\} \\
= \; & -\epsilon_{sbc} 4D \left[P_{bcst}^{(ij)} + P_{bcst}^{(ji)} \right] E_{st}.
\end{aligned}
\tag{38}
$$

In the PF case, the resulting equations differ from (38) in a few terms, which are the only ones written:

$$
\begin{aligned}
& 2 \left\{ - \left[I_{rt}^{(ij)} + I_{rt}^{(ji)} + 2K_{rt}^{(ji)} \right] \left(\tilde{u}_t^{(i)} - \tilde{u}_t^{(j)} \right) - \ldots \right\} \\
+ \; & \epsilon_{sbc} D \left\{ \left[J_{brs}^{(ij)} - J_{brs}^{(ji)} + 2n_b^{(ij)} K_{rs}^{(ij)} \right] \left(\tilde{\omega}_c^{(i)} + \tilde{\omega}_c^{(j)} \right) - \ldots \right\} \\
= \; & \ldots, \\
& 2\epsilon_{sbc} \left\{ - \left[J_{bct}^{(ij)} - J_{bct}^{(ji)} + 2n_b^{(ij)} K_{ct}^{(ij)} \right] \left(\tilde{u}_t^{(i)} - \tilde{u}_t^{(j)} \right) - \ldots \right\} \\
+ \; & \epsilon_{sbv} \epsilon_{drc} D \left\{ \left[P_{bvdr}^{(ij)} + P_{bvdr}^{(ji)} + 2n_b^{(ij)} K_{vd}^{(ij)} n_r^{(ij)} \right] \left(\tilde{\omega}_c^{(i)} + \tilde{\omega}_c^{(j)} \right) - \ldots \right\} \\
= \; & \ldots.
\end{aligned}
\tag{39}
$$

On the other hand, if the equations of force balance and those of torque balance are, in turn, summed to and subtracted from each other, one obtains in the 1FP case:

$$
\begin{aligned}
& 2 \left\{ - \left[I_{rt}^{(ij)} - I_{rt}^{(ji)} \right] \left(\tilde{u}_t^{(i)} - \tilde{u}_t^{(j)} \right) - \left[I_{rt}^{(ij)} + I_{rt}^{(ji)} \right] \left(\tilde{u}_t^{(i)} + \tilde{u}_t^{(j)} \right) \right\} \\
+ \; & \epsilon_{sbc} D \left\{ \left[J_{brs}^{(ij)} + J_{brs}^{(ji)} \right] \left(\tilde{\omega}_c^{(i)} + \tilde{\omega}_c^{(j)} \right) + \epsilon_{sbc} D \left[J_{brs}^{(ij)} - J_{brs}^{(ji)} \right] \left(\tilde{\omega}_c^{(i)} - \tilde{\omega}_c^{(j)} \right) \right\} \\
= \; & -4D \left[J_{crs}^{(ij)} + J_{crs}^{(ji)} \right] E_{sc}, \\
& 2\epsilon_{sbc} \left\{ - \left[J_{bct}^{(ij)} + J_{bct}^{(ji)} \right] \left(\tilde{u}_t^{(i)} - \tilde{u}_t^{(j)} \right) - \left[J_{bct}^{(ij)} - J_{bct}^{(ji)} \right] \left(\tilde{u}_t^{(i)} + \tilde{u}_t^{(j)} \right) \right\} \\
+ \; & \epsilon_{sbv} \epsilon_{drc} D \left\{ \left[P_{bvdr}^{(ij)} - P_{bvdr}^{(ji)} \right] \left(\tilde{\omega}_c^{(i)} + \tilde{\omega}_c^{(j)} \right) + \left[P_{bvdr}^{(ij)} + P_{bvdr}^{(ji)} \right] \left(\tilde{\omega}_c^{(i)} - \tilde{\omega}_c^{(j)} \right) \right\} \\
= \; & -\epsilon_{sbc} 4D \left[P_{bcst}^{(ij)} - P_{bcst}^{(ji)} \right] E_{st},
\end{aligned}
\tag{40}
$$

while in the PF case:

$$
\begin{aligned}
& 2\left\{... - \left[I_{rt}^{(ij)} + I_{rt}^{(ji)} - 2K_{rt}^{(ij)}\right]\left(\tilde{u}_t^{(i)} + \tilde{u}_t^{(j)}\right)\right\} \\
+\ & \epsilon_{sbc}D\left\{... + \epsilon_{sbc}D\left[J_{brs}^{(ij)} - J_{brs}^{(ji)} - 2n_b^{(ij)}K_{rs}^{(ij)}\right]\left(\tilde{\omega}_c^{(i)} - \tilde{\omega}_c^{(j)}\right)\right\} \\
=\ & ..., \\
& 2\epsilon_{sbc}\left\{... - \left[J_{bct}^{(ij)} - J_{bct}^{(ji)} - 2n_b^{(ij)}K_{ct}^{(ij)}\right]\left(\tilde{u}_t^{(i)} + \tilde{u}_t^{(j)}\right)\right\} \\
+\ & \epsilon_{sbv}\epsilon_{drc}D\left\{... + \left[P_{bvdr}^{(ij)} + P_{bvdr}^{(ji)} - 2n_b^{(ij)}K_{vd}^{(ij)}n_r^{(ij)}\right]\left(\tilde{\omega}_c^{(i)} - \tilde{\omega}_c^{(j)}\right)\right\} \\
=\ & ....
\end{aligned}
\tag{41}
$$

Comparison between equations (38) and (39) on one side, and (40) and (41) on the other shows that the 1FP and the PF approach differ only in the isolated contribution from the chosen contact ij. Our calculations prove that this contribution has a stiffening effect on the behavior of the equivalent continuum.
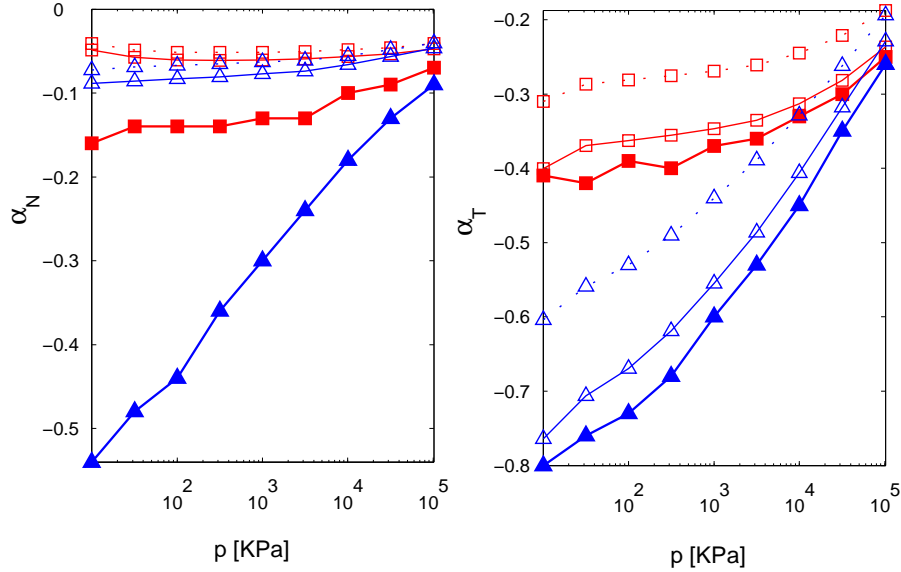

Figure 10: Estimated and measured value of α_N and α_T for sample A($\square$) and C($\triangle$). Filled symbols: measured values; empty symbols and dotted line: PF estimate; empty symbols and solid line: 1FP estimate.

Additional information about the way this contribution enters the macroscopic behavior in the 1FP and FP model can be inferred once an averaging process has been applied on the solving equations. To this aim, use is made of the main findings in section 5, where it has been shown that only the average of the fluctuations over equally oriented contacts is relevant to the macroscopic behavior; that this average is determined by the average structure of the assembly, and, finally, that such an

average structure depends on the average contact stiffness and the average geometry. On this base, it is feasible to substitute the local structural sums in (38), (39), (40) and (41) with their average over contacts with the same solid angle. As a result, the equations will give the average displacement over equally oriented contacts. We find it convenient to introduce the notation:

$$
\begin{aligned}
\overline{I}_{rt}^{(ij)} &= \langle K_N \rangle \, n_r^{(ij)} n_t^{(ij)} + \langle K_T \rangle \left(\delta_{rt} - n_r^{(ij)} n_t^{(ij)} \right) \\
&+ \langle K_N \rangle \langle \sum_{a=1,a\neq j}^{N(i)} n_r^{(ia)} n_t^{(ia)} \rangle + \langle K_T \rangle \langle \sum_{a=1,a\neq j}^{N(i)} \left(\delta_{rt} - n_r^{(ia)} n_t^{(ia)} \right) \rangle, \\
\overline{J}_{rts}^{(ij)} &= \langle K_N \rangle \, n_r^{(ij)} n_t^{(ij)} n_s^{(ij)} + \langle K_T \rangle \, n_r^{(ij)} \left(\delta_{ts} - n_t^{(ij)} n_s^{(ij)} \right) \\
&+ \langle K_N \rangle \langle \sum_{a=1,a\neq j}^{N(i)} n_r^{(ia)} n_t^{(ia)} n_s^{(ia)} \rangle \\
&+ \langle K_T \rangle \langle \sum_{a=1,a\neq j}^{N(i)} n_r^{(ia)} \left(\delta_{ts} - n_t^{(ia)} n_s^{(ia)} \right) \rangle, \\
\overline{P}_{rtsg}^{(ij)} &= \langle K_N \rangle \, n_r^{(ij)} n_t^{(ij)} n_s^{(ij)} n_g^{(ij)} + \langle K_T \rangle \, n_r^{(ij)} \left(\delta_{ts} - n_t^{(ij)} n_s^{(ij)} \right) n_g^{(ij)} \\
&+ \langle K_N \rangle \langle \sum_{a=1,a\neq j}^{N(i)} n_r^{(ia)} n_t^{(ia)} n_s^{(ia)} n_g^{(ia)} \rangle \\
&+ \langle K_T \rangle \langle \sum_{a=1,a\neq j}^{N(i)} n_r^{(ia)} \left(\delta_{ts} - n_t^{(ia)} n_s^{(ia)} \right) n_g^{(ia)} \rangle, \quad (42)
\end{aligned}
$$

where the average structural sums have been overbarred. These objects are tensors, and in the presence of isotropy, their representation is identical for all contact orientations in the local reference frame of $(\mathbf{n}^{(ij)}, \mathbf{t}^{E(ij)}, \tilde{\mathbf{t}}^{(ij)})$, where $\tilde{\mathbf{t}}^{(ij)}$ is the unit tangent vector perpendicular to $\mathbf{n}^{(ij)}$ and $\mathbf{t}^{E(ij)}$. Moreover, due to symmetry,

$$
\overline{I}_{rt}^{(ij)} = \overline{I}_{rt}^{(ji)}, \quad \overline{J}_{rts}^{(ij)} = -\overline{J}_{rts}^{(ji)}, \quad \overline{P}_{rtsg}^{(ij)} = \overline{P}_{rtsg}^{(ji)},
$$

which reduce equations (38) to

$$
\begin{bmatrix} \overline{I}_{rt}^{(ij)} & \epsilon_{sbc} D \overline{J}_{brs}^{(ij)} \\ \epsilon_{sbr} \overline{J}_{brt}^{(ij)} & \epsilon_{sbv} \epsilon_{drc} \overline{P}_{bvdr}^{(ij)} \end{bmatrix} \begin{bmatrix} -2\left(\tilde{u}_t^{(i)} - \tilde{u}_t^{(j)} \right) \\ \tilde{\omega}_c^{(i)} + \tilde{\omega}_c^{(j)} \end{bmatrix} = \begin{bmatrix} -4D \overline{J}_{crs}^{(ij)} E_{sc} \\ -4D^2 \epsilon_{sbc} \overline{P}_{bcst}^{(ij)} E_{st} \end{bmatrix}, \quad (43)
$$

and equations (39) to a system whose known terms are the same as in (43), but whose solving matrix:

$$
\begin{bmatrix} \overline{I}_{rt}^{(ij)} + \langle K_{rt} \rangle & \epsilon_{sbc} D \left(\overline{J}_{brs}^{(ij)} + n_b^{(ij)} \langle K_{rs} \rangle \right) \\ \epsilon_{sbr} \left(\overline{J}_{brt}^{(ij)} + n_b^{(ij)} \langle K_{rt} \rangle \right) & \epsilon_{sbv} \epsilon_{drc} \left(\overline{P}_{bvdr}^{(ij)} + n_b^{(ij)} \langle K_{vd} \rangle n_r \right) \end{bmatrix} \quad (44)
$$

still differs from (43) in the isolated contributions from the chosen contact ij. Finally, the averaging process reduces equation (40) to

$$
\begin{bmatrix}
\overline{I}_{rt}^{(ij)} & \epsilon_{sbc}D\overline{J}_{brs}^{(ij)} \\
\epsilon_{sbc}\overline{J}_{bct}^{(ij)} & \epsilon_{sbv}\epsilon_{drc}D\overline{P}_{bvdr}^{(ij)}
\end{bmatrix}
\begin{bmatrix}
-2\left(\tilde{u}_t^{(i)} + \tilde{u}_t^{(j)}\right) \\
\tilde{\omega}_c^{(i)} - \tilde{\omega}_c^{(j)}
\end{bmatrix}
=
\begin{bmatrix}
0 \\
0
\end{bmatrix},
$$

which differs from the average of equations (41) only in the solving matrix:

$$
\begin{bmatrix}
\overline{I}_{rt}^{(ij)} - \langle K_{rt}\rangle & \epsilon_{sbc}D\left(\overline{J}_{brs}^{(ij)} - n_b^{(ij)}\langle K_{rs}\rangle\right) \\
\epsilon_{sbc}\left(\overline{J}_{bct}^{(ij)} - n_b^{(ij)}\langle K_{ct}\rangle\right) & \epsilon_{sbv}\epsilon_{drc}D\left(\overline{P}_{bvdr}^{(ij)} - n_b^{(ij)}\langle K_{vd}\rangle n_r\right)
\end{bmatrix}.
$$

With respect to (38), (39), (40) and (41), the average contribution from the chosen contact emerges more neatly. Equations (43) and (44) are sufficient to determine the elastic moduli, as they can be solved for the average relative displacements that do contribute to the contact forces. As $\tilde{u}_t^{(i)} + \tilde{u}_t^{(j)}$ and $\omega_b^{(i)} - \omega_b^{(j)}$ do not contribute to (43) and (44), the average total force and torque the neighbors exert on the pair as a result of its rolling and of its rigid motion are zero in these approximation schemes. The reader is referred to (Bagi and Kuhn, 2004) and (Kuhn and Bagi, 2004) for a review of recent results about rolling in granular media, which is deferred for future work.

The remaining step towards a continuum equivalent description would consist in the search for an appropriate analytical formulation of (43) and (44). As far as the PF scheme is concerned, two formulations are proposed, in Jenkins et al (2005) for spheres and in Agnolin et al. (2005) for disks. However, those both consider the isolated contributions from the contact ij in (44) of the second order and neglect it, and thus correspond to the 1FP case. In more general terms, the key element to the analytical formulation is the choice of appropriate distribution functions for the contact orientation, which allow to transform the structural sums into integrals. As already noticed by Jenkins (1997), such a choice cannot stem from the focus on the individual particle alone, as in this case symmetry in the contact distribution would make the third order tensor J_{rst} in (42) be zero. If the third order tensor were zero, from (43) the center displacements would be zero as well, and rotations would balance alone the effect of a biaxial load, in contradiction to both experiments and numerical simulations. Therefore, adequate statistical representations of the average structure need to incorporate considerations of impenetrability between neighboring particles. On this base, Jenkins (1997) concluded on the inadequacy of the 1FP approach and later on introduced the PF method, while here it has been proven that the 1FP approach is already effective in capturing the fluctuations, at the condition that the focus be extended to the pair.

7   Conclusions and perspectives

Four numerical isotropic assemblies of frictional spheres have been created by employing different preparation procedures. Of these, the first one is the classic frictionless

isotropic compression; two procedures aim to reproduce compaction by vibration and lubrication, respectively, while the fourth one is a frictional compression. The coordination number of the four samples obtained in this way is found to strongly vary with the preparation procedure, and their elastic moduli depend much more on coordination number than on density. The initial states of the first three samples all match in pressure and density that of assemblies of glass beads used during a series of wave propagation experiments, but as far as the elastic moduli are concerned, only those of the low-coordinated sample produced by the protocol aimed at mimicking vibration match the experimental results satisfactorily at pressures lower than 1 MPa. Conversely, samples created by means of an initial isotropic compression, the scientific literature usually focuses on, are far too stiff in this range of pressure.

The interest of Continuum Mechanics research is in the prediction of the mechanical properties, which requires that of the relative displacement between contacting grains. In these respects, the easiest scenario possible is that of relative displacements driven by the average strain. Such an hypothesis results in poor estimates of the shear modulus, which indicates the necessity of incorporating the displacement fluctuations from the average strain. We have found that the fluctuations chiefly depend on coordination number. Locally, the fluctuations vary strongly, as they ensure the balance of force and torque at the grain scale, but only their average over contacts with the same orientation affects the macroscopic behavior. This average is determined by the average geometry and the average contact stiffness. In more detail, the average normal and tangential component of the contact displacements induced by the fluctuations are proportional, in turn, to the normal and the tangential relative displacement induced by the average strain. Along the tangential direction, the relaxation with respect to the average strain assumption is generally entirely due to rotations; the tangential fluctuations of the centers give a much smaller contribution, and mainly originate in the requirement of local equilibrium.

Displacement fluctuations consistent with these observations result from the 1FP and the PF approach, which have been promisingly employed in the past to predict the moduli of frictionless spheres and frictional disks, and which have been tested numerically on our assemblies of frictional spheres. In this way, the bound has been identified which can be attained by the corresponding analytical solutions for frictional spheres. Both approaches are based on the equilibrium of a small subassembly made, in turn, of a particle and a pair of contacting grains with their first neighbors. The chosen particle or pair alone is allowed to fluctuate, while the neighborhood move in accordance with the average strain. Both approaches result in a remarkable improvement of the estimate of the shear modulus with respect to the average strain assumption, meaning that the fluctuations which mostly affect the macroscopic behavior correlate over a short lenght. The estimate is satisfying in the case of samples with large coordination number, and optimal predictions for samples with a smaller coordination number are likely to result from just incorporating the fluctuations of the first neighbors. Tangential fluctuations are rather satisfactorily captured, and the residual discrepancy between predicted and effective shear modulus is mostly due to the underestimate of radial fluctuations.

References

Agnolin, I., Roux J.-N., Massaad, X.J., Jia, X., Mills, P., 2005. Sound wave velocities in dry and lubricated granular packings: numerical simulations and experiments. In: Garcia-Rojo, R., Hermann H.J., McNamara, S. (Eds.), Powders and Grains 2005. Balkema Publishers, Rotterdam, 313-317.

Agnolin, I., Jenkins, J.T., La Ragione L., 2006. A continuum theory for a random array of identical, elastic, frictional disks. Mechanics of Materials 38, 687-701.

Agnolin, I., Kruyt, N.P. 2006. On the elastic moduli of two-dimensional assemblies of disks: relevance and modelling of fluctuations in particle displacements and rotations. Accepted for publication in: Computers and Mathematics with Applications.

Agnolin, I., Roux, J.-N., 2007. Isotropic granular packings: internal state and elastic properties. Submitted.

Aste, T., Saadaftar, M., Senden, T.J., 2005. Geometrical structure of disordered sphere packings. Physical Review E 71, 061302.

Atman, A.P.F., Brunet, P., Geng, J., Reydellet, G., Combe, G., Claudin, P., Behringer, R.P., Clement, E., 2005. Sensitivity of the stress response function to packing preparation.

Bagi, K., Kuhn, M.R., 2004. A definition of particle rolling in a granular assembly in terms of particle translations and rotations. Journal of applied mechanics 71, 493-501.

Calvetti, F., Emeriault, F., 1999. Interparticle force distribution in granular materials: link with the macroscopic behavior. Mech. Cohes.-Frict. Mater. 4, 247-279.

Chang, C.S., Chao, S.J., Chang, Y., 1995. Estimates of elastic moduli for granular material with anisotropic random packing structure. Int. J. Solids Structures 32, 1989-2008.

Cundal, P.A., Strack, O.D.L., 1979. Discrete numerical model for granular assemblies. Geotechnique 29, 47-65.

Cundall, P.A., Jenkins, J.T., Ishibashi, I., 1989. Evolution of elastic moduli in a deforming granular assembly. In: Biarez , Gourves (Eds.), Powders and Grains 1989. Balkema Publishers, Rotterdam, 319-322.

Cundall, P.A., Strack, O.D.L., 1983. Modeling of microscopic mechanisms in granular materials. In: Jenkins & Satake (eds.), Mechanics of granualar materials: new models and constituive relations. 137-149. Amsterdam: Elsevier.

da Cruz, F., Emam, S., Prochnow, M., Roux, J.-N., Chevoir, F., 2005. Rhephysics

of dense granular materials: discrete simulation of plane shear flows. Physical Review E, 021309-021326.

Digby, P.J., 1981. The effective elastic moduli of porous granular rocks. J. of Applied Mechanics 48, 803-808.

Domenico, S.N., 1977. Elastic properties of unconsolidated porous reservoirs, Geophysics 42(7), 1339-1368.

Drescher, A., de Josselin de Jong, G., 1972. Photoelastic verification of a mechanical model for the flow of a granular material. J. Mech. Phys. Solids 20, 337-351.

Duffy, J., Mindlin, R.D., 1957. Stress-strain relations and vibrations of a granular medium. ASME J.Applied Mechanics 24, 585-593.

Elata, D., Berryman, J.G., 1996. Contact force-displacement laws and the mechanical behavior of random packs of identical spheres. Mech. of Materials 24, 229-240.

Gaspar, N., Koenders, M.A., 2001. Micromechanic formulation of macroscopic structures in a granular medium. J. Engineering Mech. 127, 987-992.

Goddard,J., 1990. Nonlinear elasticity and pressure-dependent wave spedds in granular media. Proc. R. Soc. Lond. A 430, 105-131

Hicher, P.Y., 1996. Elastic properties of soils. ASCE Journal of Geotechnical Engineering 122, 641-648.

Jenkins, J.T., 1997. Inelastic behavior of random arrays of identical spheres. In: Fleck, N.A., 5Ed., Mechanics of Porous and Granular Materials. Kluwer: Amsterdam, 11-22.

Jenkins, J.T., La Ragione, L., 2001. Fluctuations and state variables for random arrays of identical spheres. In: Kishino, Y. (Eds.), Powders and Grains 2001, Balkema Publishers, Rotterdam, 195-198.

Jenkins, J.T., Johnson, D., La Ragione, L., Makse, H., 2005. Fluctuations and the effective moduli of an isotropic, random aggregate of identical, frictionless spheres. Int. J. Mechanics and Physics of Solids 53, 197-225.

Jia, X., Mills, P., 2001. Sound propagation in dense granular materials. In: Kishino, Y. (Eds.), Powders and Grains 2001, Balkema Publishers, Rotterdam, 105-112.

Johnson, K.L., 1985. In: Contact Mechanics. Cambridge University Press.

Johnson, D.L., Norris, A.N., 1996. Rough elastic spheres in contact: memory effects and the transverse force. Int. J. Mechanics and Physics of Solids 45, 1025-1036.

Koenders, M.A., 1987. The incremental stiffness of an assembly of particles. Acta Mechanica 70, 31-49.

Kruyt, N.P., Rothenburg, L., 2001. Statistic of the elastic behavior of granular materials. International J. of Solids and Structures 38, 4879-4899.

Kruyt, N.P., Rothenburg, L., 2002. Micromechanical bounds for the effective elastic moduli of granular materials. International J. of Solids and Structures 39, 311-324.

Kuhn, M.R., 1999. Structured deformation in granular materials. Mech. of Materials 31, 407-429.

Kuhn, M.R., Bagi, K., 2004. Contact rolling and deformation in granular media. International Journal of Solids and Structures 41, 5793-5820.

Love, A.E.H, 1944. In: A treatise on the mathematical theory of elasticity, Appendix B. New York Dover Publications.

Mindlin, R.D., Deresiewicz, H., 1953. Elastic spheres in contact under varying oblique forces. J. Appl. Mech. 20, 327-344.

Makse, H.A., Gland, N., Johnson, D.L., Schwartz, L., 2004. Granular packings: nonlinear elasticity, sound propagation, and collective relaxation dynamics. Physical Review E 70,061302.

Majmudar, T., Behringer, R., 2005. Contact force measurements and stress-induced anisotropy in granular materials. Nature 435, 1079-1082.

Nicolas, M., Duru, P., Pouliquen, O., 2000. Compaction of a granular material under cyclic shear. European Physics J. E 3, 309-314.

Procopio, A.T., Zavanglios, A., 2005. Simulations of multi-axial compaction of granular media from loose to high relative densities. J. Mech. and Physics of Solids 53(7), 1523-1551.

Roux J.-N., 2000. Geometric origin of mechanical properties of granular materials. Physical Review E 61, 6802-6836.

Thomann, T.G., Hryciw, R.D., 1990. Laboratory measurement of small shear strain shear modulus under K_o conditions. ASTM Geotechnical Testing Journal 13, 97-105.

Thornton, C., 2000. Numerical simulations of deviatoric shear deformation of granular media. Geotechnique 50, 43-53.

Thornton,C., Antony, S.J., 1998. Quasi-static deformation of particulate media. Phil. Trans. R. Soc. London A 356, 2763-2782.

Trentadue, F., 2003. An equilibrium-based approach for the micromechanical modelling of a non-linear elastic granular material. Mech. of Materials 36, 323-334.

Velicky, B., Caroli, C., 1999. Pressure dependence of the sound velocity in a two-dimensional lattice of Hertz-Mindlin balls: mean-field description. Physical review E 65, 021307, 1-14.

Walton, K., 1987. The effective elastic moduli of a random packing of spheres. Journal of the Mechanics and Physics of Solids 35, 213-226.

Williams, J.R., Rege, N., 1997. Coherent vortex structures in deforming granular materials. Mechanics of Cohesive-Frictional Materials 2, 223-236.